1

# Modeling of Two-Dimensionally Maneuverable Jellyfish-Inspired Robot Enabled by Multiple Soft Actuators

Shengbin Wang and Zheng Chen\*

Abstract—Soft actuators, such as dielectric elastomer (DE) and ionic polymer metal composite (IPMC), can generate large deformation under electric stimuli, which makes them promising in bio-mimetic robotic jellyfish applications. Although dielectric elastomers and ionic polymer metal composites (IPMCs) have been used in jellyfish-inspired robots respectively, there is no research which combines both of them to develop a jellyfish robot capable of two-dimensionally (2D) maneuvering capability. In our previous work, a jellyfish robot fabricated with DE can achieve effective locomotion. However, the robot requires a big bell to provide propulsion and can only move vertically. The jellyfish-inspired robot developed in this paper exhibits contracting muscle-like behaviour using a DE membrane to generate a periodic contraction on its eight fins to provide a thrust force which propels the robot to transit through underwater. The robot utilizes an IPMC to generate a bending moment which directs the heading angle of its swimming. This paper presents the design, modeling, experimental characterization of the 2D maneuverable jellyfish robot. The preliminary results show the jellyfish-inspired robot can swim underwater effectively in the vertical direction with different sinusoidal input signals, the direction of the robot can be changed by bending the IPMC. The average speed of the robot is about 4.8 mm/s when a sinusoidal signal with 5 kV amplitude and 1.4 Hz frequency is applied to the DE actuator. The maximum average heading angle change can reach to 3.02° by actuating IPMC without voltage applied to DE.

Index Terms—Biologically-inspired Robots, Marine Robotics, Soft Robot Materials and Design

#### I. Introduction

TNDERWATER microrobots with multiple degrees of freedom, that can walk and swim freely in water are important topics in the field of ocean monitoring for applications such as pollution detection and video mapping without causing unintentional damage to fragile objects [1]. Among the fascinating aquatic animals, jellyfish can be categorized to be one of the best choices for their energy efficiency, axisymmetric morphology, low metabolic rate, etc [2]. Compared to conventional rigid underwater vehicles with large power consumption and propellers or jet thrusters which generate considerable vibration and noise, soft robotic fishes have tremendous advantages in exploring and monitoring delicate marine ecosystems and are better able to adapt to uncertain circumstances [3] [4]. The unique appearance of the jellyfish

Shengbin Wang and Zheng Chen are with the Department of Mechanical Engineering, University of Houston, 4800 Calhoun Rd, Houston, TX 77004. (e-mail: swang62@uh.edu (SW); zchen43@central.uh.edu) (ZC)

and its swimming behaviour make the jellyfish-inspired robots be an interesting topic for the researchers in bio-inspired robotics [5]. The significant potential for developing the jellyfish robot will help us build a tool to monitor and explore marine resources.

Some jellyfish-inspired robots have been developed, such as light-driven jellyfish robot [6], pumps driven jellyfish robot [7]. The key to imitating jellyfish-like morphology and movement is to produce thrust force to push the jellyfish to move forward [8], which can be achieved with the help of smart materials. One of the most popular materials used to develop the jellyfish robot is ionic polymer metal composite (IPMC) which can exhibit large dynamic deformation with the varying electric field [9]. The bending motion is caused by the motion of the moving cations inside of the polymer matrix. Many researchers developed IPMC enabled jellyfish robots where IPMCs provide actuation power and expand the deflection of the bell [10] [11]. Joseph et al. developed a new jellyfishlike microrobot using eight IPMC actuators to achieve a bioinspired bell kinematics design [12]. However, the slow time response of IPMC causes a low contraction frequency on the bell, thus the maximum speed of IPMC enabled jellyfish is limited [13].

Another promising candidate for developing bio-inspired jellyfish robot is dielectric elastomer (DE). The biomimetic underwater jellyfish robots made with DE material combine many appealing features such as high compliance around 1 MPa [14], fast response less than 200  $\mu$ s [15], and the self-sensing capacity [16] [17]. Some methods of fabricating jellyfish robots with DE material have been proposed. An untethered jellyfish inspired soft robot was developed with an axisymmetric array of unimorph actuator [18], one challenge of this jellyfish is to improve the speed of the robot to work in high flow environments. Hareesh et al. [19] developed a jellyfish robot with chamber structure made with DE material, simplified integrated design for fabrication and untethered soft robotic jellyfish by DE material was proposed by Tingyu, et al. [20]. However, the speed of the jellyfish is limited and the propulsion to push the jellyfish to move forward is mostly restricted by the DE actuator in their research. Besides, it is difficult to change the movement direction of the robots.

To tackle the aforementioned inadequacies associated with jellyfish robots, a novel jellyfish robot fabricated with multiple DE membranes and IPMC is introduced in this paper. This is the first time combing DE and IPMC to generate thrust force to make the jellyfish move upward and change the direction.

<sup>\*</sup> Corresponding author: Zheng Chen. This work was supported by the National Science Foundation under Grant CMMI #1747855.

DE is an ideal material to provide large deformation and can withstand high frequencies. Compared to DE, IPMC does not need to be pre-stretched and it can generate a bending moment which directs the heading angle of swimming jellyfish. The positive electrode of the DE is enclosed between the two membranes, the negative electrode is directly exposed to water since the surrounding water serves as a ground electrode. This paper also describes a simplified modeling approach which can capture the major components in the model.

The structure of this paper is arranged as following: Section II introduces the design and fabrication of the jellyfish robot, Section III provides simplified DE membrane actuation model and heading angle model, Section IV shows some preliminary experimental results including both frequency response and swimming speed characterization. Section V discusses the conclusion of the paper and the future research for this jellyfish robot.

#### II. DESIGN AND FABRICATION

The new jellyfish robot is fabricated based on our previous jellyfish robot [21]. Previous works show different execution mechanisms with contraction from a complete bell. The current jellyfish robot produces thrust force with the eight fins. Furthermore, the present work achieved 2D maneuvering capability by bending the IPMC. The jellyfish robot is composed of the following four parts.

#### A. Actuation System

The DE membrane provides deformation to actuate the movement of the fins, which is fabricated with 300% prestretching 3M VHB 4910 membrane with compliant electrodes (carbon powder). The diameter of the bell is 120 mm, consisting of 8 fins. The diameter of the DE membrane is also 120 mm, which is same with our previous jellyfish robot. A bigger O-ring is designed to connect the DE actuator and bell, as shown in Fig. 1. In order to avoid the bubbles being isolated between DE membrane and big O-ring, four fan-shaped holes are cut on the surface of the big O-ring.

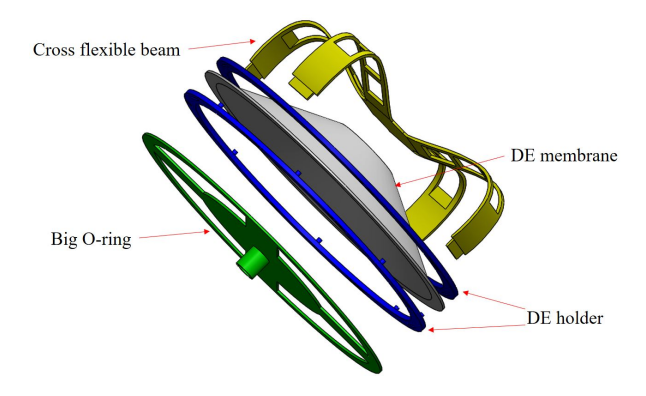


Fig. 1: Assembly of the DE actuator.

When a sinusoidal voltage wave is applied on the DE membrane, the electrical field cross the DE membrane is transduced to a Maxwell stress which causes the DE membrane

to decrease in thickness and increase in area. The spring-like cross flexible beam pulls the DE membrane to move up and down, which causes eight fins to swing and produce propulsion. The schematic of this procedure is shown in Fig. 2. The IPMC will bend when a constant voltage is applied on it, the position of the foam on the top of the IPMC will be changed. The body of the jellyfish robot tilts, which in turn changes the heading angle of robot.

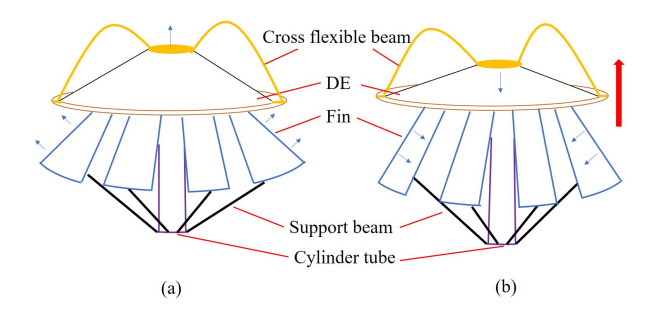


Fig. 2: The schematic of moving jellyfish: (a) maximum voltage (b) minimum voltage.

# B. Moving Structure

The eight fins of the jellyfish robot are connected as shown in Fig. 3, which will be pushed to swing by the movement of DE membrane, provides thrust force to drive the jellyfish to swim. To improve movement stability, all of the fins are fixed to the bottom of the big O-ring with VHB tape and silicon glue.

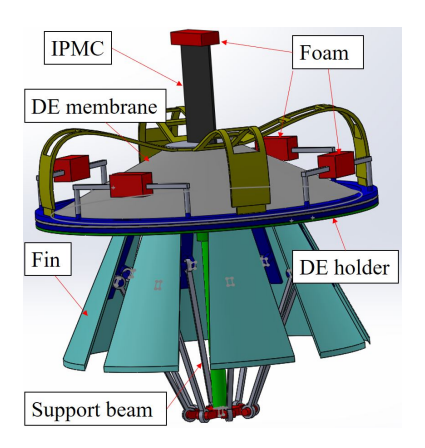


Fig. 3: Assembly of the jellyfish robot.

# C. Support Stands

To hold the DE membrane and the cross flexible beam together, the upper middle of the DE membrane will be used as the linking agency, which can provide strong adhesion to the cross beam. A cylinder tube is fixed in the middle of the bottom of the DE, which can hold the eight support beams and transmit the movement of the DE to the eight fins. All connections between the support beam and the other parts are hinged, so they can rotate around their respective axes.

#### D. Buoyancy Adjustment

There are two buoyancy adjustment systems for this jellyfish robot as shown in Fig. 3. The first one is used to adjust the whole body of the robot, and keep it perpendicular to the bottom. Four foams with their own beams are assembled on the DE holder. By increasing or decreasing the size of the foam manually, the buoyancy of the whole jellyfish body will be equal to its weight or just less than its weight a little bit to bring negative buoyancy. By moving the position of each foam, the final jellyfish robot can manipulate accordingly towards desired direction at targeted angles. The jellyfish will be adjusted to be perpendicular to the bottom of the water tank at the beginning of the experiment. The second buoyancy adjustment system is IPMC. By adjusting the bending angle of the IPMC, the jellyfish robot can change its moving direction.

#### III. MODELING OF THE JELLYFISH ROBOT

# A. DE Membrane Actuation Model

The vertical pre-stretching of the DE membrane is supported by the flexible cross beam which is a 'negative-rate bias spring' or NBS, and a promising bias element when using in high-performance DE actuator [22]. The cross beam is simplified into a linear spring in this paper. The maximize displacement we can get is h without destroying its structure, and the maximize force is F. Then according to Hooke's law F = kh, the spring constant k is obtained.

The theoretical analysis based on the fabricated jellyfish robot provides simulation results and explains how the jellyfish moves with its actuation when the electric power is applied on the DE. Fig. 4 shows the sectional view of the DE actuator, the description process of the simplified frustum DE actuator is shown on the left side. The original state without applied voltage and vertical pre-stretching is shown on the upper side of Fig. 4. The origin of coordinate axis system is built in the center of the circular frame to show the movement of the middle plate. A and B are the edges of the inner and outer of the circle support respectively. The radius of the middle plate is *a*, and the radius of the outside DE membrane is *b*.

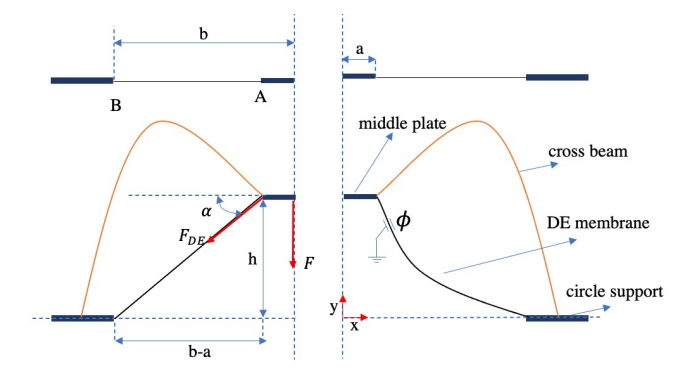


Fig. 4: Sectional view of DE actuator.

The acceleration of the middle plate can be obtained when the height of the cross beam and input voltage applied on the DE membrane such parameters are given. See our previous paper [21] for further details.

$$\begin{split} \ddot{h} &= \frac{1}{m} \{ \bar{k} (H - h) - 4 \pi r (\frac{b - a}{\sqrt{(b - a)^2 + h^2}} \frac{r_0}{r_p}^2 z_0) \\ &\frac{h}{\sqrt{h^2 + (b - a)^2}} u [(\frac{r_p}{r_0} \frac{\sqrt{(b - a)^2 + h^2}}{b - a})^2 \\ &- (\frac{r_p}{r_0} \frac{\sqrt{(b - a)^2 + h^2}}{b - a})^{-2} (\frac{r_p}{r_0})^{-2} ] \\ &- \varepsilon ((b - a)^2 + h^2) (\frac{V}{z_p (b - a)})^2 - mg - c\dot{h} \}. \end{split} \tag{1}$$

The fin contracts and relaxes through the transmission mechanism powered by the movement of the DE membrane. Assuming that the fin is an ideal elastomer with a isosceles trapezoid shape. The outline of the eight fins can be treated as a conical frustum. The radius of the top surface remains the same, while the bottom radius and the height of the conical frustum change when the eight fins swing. Fig. 5 shows the half of 2D section view of the simplified conical frustum, where the solid line is the original state of one fin of the jellyfish and the dashed line is the final state. The thrust force generated by the fins depends on the angle change of the eight fins.

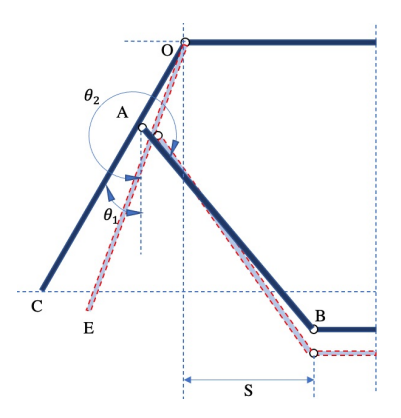


Fig. 5: Simplified fin shape with conical frustum.

The structure from the transmission part to the fin is equal to the offset slider-crank mechanism which can be used for velocity and acceleration analysis for the eight fins effectively. The movement of point B is limited in the vertical direction, which is equal to the slider. OA can rotate around the point O, and OAB is similar to the crank, S is the offset length. Assuming the angular velocity of the fin is constant during each period of swinging, the angular acceleration is considered to be 0. Some parameter functions can be built based on our previous research [21], the acceleration of point O can be calculated as below:

$$\begin{split} a_{B} &= -l_{OA}\omega_{1}^{2}\cos\theta_{1} - l_{AB}(\frac{-l_{OA}\omega_{1}\cos\theta_{1}}{l_{AB}\cos\theta_{2}})^{2}\cos\theta_{2} \\ &- (\frac{l_{OA}\omega_{1}^{2}\sin\theta_{1}}{\cos\theta_{2}} + \frac{\tan\theta_{2}}{l_{AB}}(\frac{-l_{OA}\omega_{1}\cos\theta_{1}}{\cos\theta_{2}})^{2})\sin\theta_{2}. \end{split} \tag{2}$$

Comparing (1) and (2),  $\ddot{h}$  is equivalent to  $a_B$ . Both of them are the acceleration of point B on vertical direction. By combining the two groups of the functions,  $\omega_1$  can be solved.

The oscillating fin is displayed in Fig. 6. There is a black rectangular plate glued to the front part of each single fin, which separates the fin into front fin and rear fin, as shown on the left of Fig. 6. The rear fin can rotate along the dividing line *GH*. The movement of both front fin and rear fin is around themselves doing pitching movement, and they are simplified as rigid fin during their movement in the uniform flow field. The propulsive force is generated from the fluctuation of the eight fins, which is produced from the momentum transfer because of the interaction between the fins and the water [23]. To simplify the model, the added mass components are ignored in the fin-fluid interaction, the contributions to the momentum transfer mechanism are due to drag and lift force.

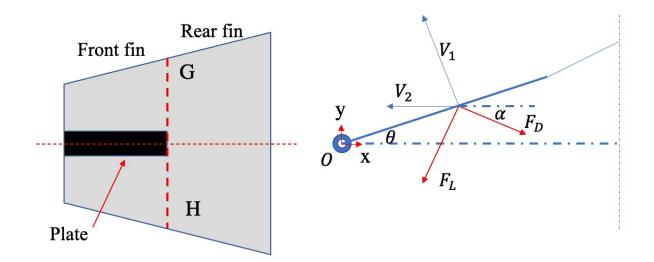


Fig. 6: Velocity and force acting on the oscillating fin.

The equation of movement of front fin can be calculated as follows [24]:

$$Y = L\sin(2\pi f t),$$
  

$$\theta = \theta_0 \sin(2\pi f t).$$
(3)

where L is the motion amplitude of the front fin, f is the oscillation frequency, and  $\theta_0$  is the corresponding pitching angular amplitude. The magnitude of the front fin speed at the chord midpoint distance can be calculated based on Law of cosines:

$$V = \sqrt{(V_1)^2 + (V_2)^2 + 2V_1 V_2 \sin \theta},$$
 (4)

 $V_1, V_2$  can be calculated with (3) as follows:

$$V_1 = 2\pi f L \cos(2\pi f t),$$
  

$$V_2 = 2r\pi f \theta_0 \cos(2\pi f t).$$
(5)

where r is the distance between fin oscillation axis to the midpoint of the front fin.

Then, the velocity of the front fin relative to the fluid with a speed of  $V_0$  can be obtained as follows:

$$V_t = \sqrt{(V)^2 + (V_0)^2}. (6)$$

The viscous forces are negligible when the jellyfish robot is moving in the flow field, only drag force and lift force will be considered for the jellyfish fin in the fin-fluid interaction situation [25]. The drag force is parallel to the instantaneous velocity vector  $\vec{V}$ , while the lift force is perpendicular to the instantaneous velocity vector  $\vec{V}$ . The formulas to calculate the drag force and lift force on the front fin in the lateral direction of fin are:

$$F_{D1} = 0.5\rho(V_t)^2 C_D S \cos(\alpha),$$
  

$$F_{L1} = 0.5\rho(V_t)^2 C_L S \sin(\alpha).$$
(7)

where  $\rho$  is the density of the fluid, S is the cross sectional area,  $\alpha$  is the angle between the vector of drag force and the x axis, as shown in Fig. 6, which can be expressed as [25]:

$$\alpha = \arctan(\frac{r\dot{\theta}cos\theta}{V_1 + r\dot{\theta}sin\theta}),\tag{8}$$

With (5), (6), (7), the total propulsion produced by the front fin can be calculated as follows:

$$F_{front} = F_{D1} + F_{L1},$$

$$= 0.5\rho(((V_1)^2 + (V_2)^2 + 2V_1V_2sin\theta) + (V_0)^2)^2C_DS\cos(\alpha) + 0.5\rho(((V_1)^2 + (V_2)^2 + 2V_1V_2sin\theta) + (V_0)^2)^2C_LS\sin(\alpha)$$
(9)

Using the similar method to analyze the propulsion produced by the rear fin. The equation of movement of rear fin can be calculated as follows:

$$Y_2 = L_2 \sin(2\pi f t),$$
  

$$\theta_2 = \theta_{20} \sin(2\pi f t + \gamma).$$
(10)

where  $L_2$  is the motion amplitude of the rear fin,  $\theta_{20}$  is the corresponding pitching angular amplitude,  $\gamma$  is the phase difference between the rear fin and the front fin. The magnitude of the rear fin speed at the chord midpoint distance can be calculated as:

$$V_2 = \sqrt{(V_{12})^2 + (V_{22})^2 + 2V_{12}V_{22}sin\theta},$$
 (11)

 $V_{12}, V_{22}$  can be calculated with (10) as follows:

$$V_{12} = 2\pi f L_2 \cos(2\pi f t),$$

$$V_{22} = 2r_2 \pi f \theta_{20} \cos(2\pi f t + \gamma).$$
(12)

where  $r_2$  is the distance between fin oscillation axis to the midpoint of the rear fin. Then, the velocity of the rear fin relative to the fluid with a speed of  $V_0$  can be obtained as follows:

$$V_{t2} = \sqrt{(V_2)^2 + (V_0)^2}. (13)$$

The formulas to calculate the drag force and lift force on the rear fin in the lateral direction of fin are:

$$F_{D2} = 0.5\rho (V_{t2})^2 C_D S_2 \cos(\alpha),$$
  

$$F_{L2} = 0.5\rho (V_{t2})^2 C_L S_2 \sin(\alpha),$$
(14)

where  $S_2$  is the cross sectional area of rear fin. From the above analysis, with (12), (13), (14), the total propulsion produced by the one fin can be calculated as follows:

$$F_{rear} = F_{D2} + F_{L2},$$

$$= 0.5\rho(((V_{12})^2 + (V_{22})^2 + 2V_{12}V_{22}sin\theta) + (V_0)^2)^2C_DS_2\cos(\alpha) + 0.5\rho(((V_{12})^2 + (V_{22})^2 + 2V_{12}V_{22}sin\theta) + (V_0)^2)^2C_LS_2\sin(\alpha).$$
(15)

Assuming the angle between the vector of force F with horizontal direction is  $\beta$ , with (9) and (15), the total thrust force produce by the eight fins in vertical direction can be calculated:

$$T = 8(F_{front}\sin\beta + F_{rear}\sin(\beta + \gamma)). \tag{16}$$

### B. Heading Angle Model

The jellyfish robot is separated into two parts as shown in Fig. 7. One is the foam on the top of the jellyfish robot with light weight, the gravity of the foam was ignored. Another one includes all the remaining parts.

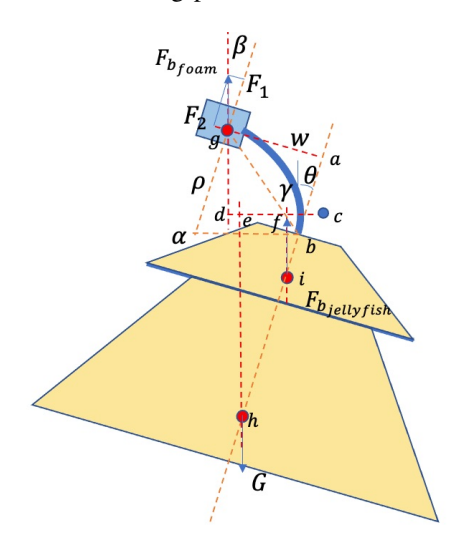


Fig. 7: Jellyfish with IPMC.

The buoyancy force  $F_{b_{foam}}$  is split into two parts, one is parallel to the central axis and another one is perpendicular to the central axis, both of them point upwards. Assuming clockwise is the positive direction, and anti clockwise is the negative direction. So the total moment of foam can be calculated below:

$$M_B = M_{B1} + M_{B2} = F_1 w + F_2 l_{ab},$$
  
=  $F_{b_{foam}} cos \beta w - F_{b_{foam}} sin \beta l_{ab}.$  (17)

where w is the distance between the center of foam buoyancy and the central axis of the robot. According to the linear beam theory, a bending equation can be given:

$$EI\frac{\partial^2 w}{\partial z^2} = M_{IPMC} - M_B, \tag{18}$$

where  $M_{IPMC}$  is the bending moment of IPMC, E is the effective Young's modulus of the IPMC, and  $I = 2/3Wh^3$  is the moment of the inertia of the IPMC. From paper [26], the bending moment of IPMC with length of  $L_0$  is obtained as:

$$M(L_0,s) = -\frac{2\alpha_0 KW k_e(\gamma(s) - tanh(\gamma(s)))\phi(h, L_0, s)}{s\gamma(s) + Ktanh(\gamma(s))}.$$
 (19)

This function performs Laplace transform for the time variable t. Where s is the Laplace variable,  $\alpha_0$  is coupling constant, K is the aggregated constant, W, h are the width and half thickness of the IPMC beam,  $k_e$  is the effective dielectric constant,  $\gamma(s) = \beta(s)h$ , and  $\beta(s)^2 = (s+K)/d$ .  $\phi$  is the electric potential. Assuming the surface electrodes are perfectly conducting on both of IPMC surface, then  $\phi(h, L_0, s) = V(s)/2$ .

When  $\frac{dw}{dx}$  is small as it is for an Euler–Bernoulli beam we can make the approximation:

$$\frac{1}{\rho} = \frac{\partial^2 w}{\partial z^2}, \ \rho \alpha = L, \ \theta \approx \frac{dw}{dx}.$$
 (20)

From Alternate Segment Theorem,  $\alpha = 2\theta$ . With (17), (18), (20), one can get:

$$2EI\frac{w}{L^2} = M_{IPMC} - F_{b_{foam}}(cos\beta w - sin\beta l_{ab}), \qquad (21)$$

The deflection of IPMC can be estimated as follows:

$$w = \frac{M_{IPMC} + F_{b_{foam}} sin \beta l_{ab}}{2\frac{EI}{12} + F_{b_{foam}} cos \beta}.$$
 (22)

The center of buoyancy and the center of gravity for the second part of the robot will keep at the same positions when the heading angle of the jellyfish robot changed. From Moment Mechanical equilibrium, when the jellyfish body with IPMC is balanced, the sum of the clockwise moments about a pivot is equal to the sum of the anticlockwise moments about the same pivot. Assume the pivot point is c. The distance between the gravity of the jellyfish body and the pivot point is ce, assume it is  $x_1$ . The distance between the buoyancy of the foam of the jellyfish body and the pivot point is cd, assume it is  $x_2$ . The distance between the buoyancy of the body of the jellyfish robot and the pivot point is cf, assume it is  $x_3$ .

$$F_{b_{foam}}x_2 + F_{b_{iellyfish}}x_3 = Gx_1. \tag{23}$$

The angle  $\angle \gamma$  can be calculated from formula below:

$$\frac{l_{bg}}{\gamma}\sin\gamma\sin\gamma = w,\tag{24}$$

Substituting (22) into (24), we obtain:

$$\frac{l_{bg}}{\gamma}\sin\gamma^2 = \frac{M_{IPMC} + F_{b_{foam}}\sin\beta l_{ab}}{2\frac{EI}{I^2} + F_{b_{foam}}\cos\beta}.$$
 (24.1)

According to the geometry structure of jellyfish, several algebraic equations can be found:

$$l_{hi}\sin\beta = x_1 - x_3,\tag{26}$$

$$l_{be}\sin(\gamma - \beta) = l_{bh}\sin\beta + (x_2 - x_1),$$
 (27)

$$(l_{ab} + l_{bh})\sin\beta = w\cos\beta - (x_2 - x_1),$$
 (28)

Inserting (22) into (28), we obtain the equation:

$$\frac{l_{bg}}{\gamma}\sin\gamma^2 = \frac{M_{IPMC} + F_{b_{four}}\sin\beta l_{ab}}{2\frac{EI}{7^2} + F_{b_{four}}\cos\beta}.$$
 (28.1)

Solve (23), (24.1), (26), (27), (28.1), one can calculate the heading angle  $\beta$  of the jellyfish robot.

# IV. EXPERIMENTAL RESULTS

# A. Frequency response of the DE membrane actuator

To determine the characteristics of the DE membrane, a system identification to estimate the transfer function of the DE actuator is performed. This is achieved by analyzing the system's frequency response of the actuator over the range of 0.02 Hz to 16 Hz with sinusoidal input signal. The full voltage range (0-5000 V) input to the DE membrane actuator is normalized between 0 to 1. The response is then plotted on the bode magnitude plot and a transfer function is fitted onto the data. The actuation voltage is provided by a high voltage

amplifier (HVA 10HVA24-BP1-F), the caliber of the cables we used for the transmission of the high voltage is 0.08 mm, the real displacement of the DE middle plate is measured with a laser sensor (Baumer OADM 20I6441/S14F), data acquisition is implemented in real-time by using Simulink and dSPACE (DS1104, dSPACE Inc.).

The magnitude of the frequency response is obtained by using Fast Fourier Transform (FFT) method. Fig. 8 shows the bode plot of the measured frequency response results. A third-order transfer function with three poles and one zero is used to fit all of the experiment data by minimizing the mean square error from the experiment data points.

$$G(s) = \frac{30740s + 153100}{s^3 + 498s^2 + 30530s + 94600}. (30)$$

The fitting accuracy of this transfer function is around 80%. Since the cut-off frequency of the transfer function is around 5 Hz, the 1 to 2 Hz actuation signals are within the actuation frequency range of the DE actuator.

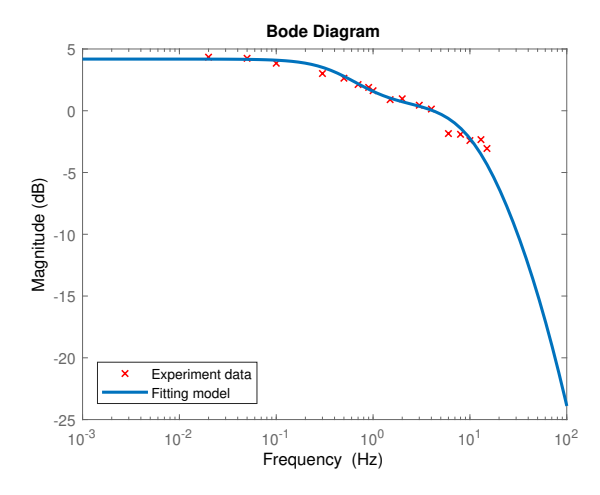


Fig. 8: Frequency response of the jellyfish actuation.

#### B. Velocity under Constant Frequency and Amplitude Signal

Six experiments are conducted using the 5 kV amplitude sinusoidal input signal and different frequency. The contraction time is equal to relaxation time for the jellyfish robot during each cycle. The experiment setup shown in Fig. 9. At the beginning of each experiment, the buoyancy of the jellyfish robot will be adjusted by the buoyancy foams to keep neutral buoyancy. The high voltage will be applied on the DE membrane after a few seconds at  $t_0$ . The jellyfish robot reaches the surface of the water pool at different times of  $t_f$ . The total spend time can be calculated by  $t = t_f - t_0$ , h is the distance the jellyfish moved, and average velocity of the jellyfish robot is

$$v = \frac{h}{t}. (31)$$

The camera is used to record the movement of the jellyfish robot, then analyzed by the computer. The experiment results are summarized in Table I.

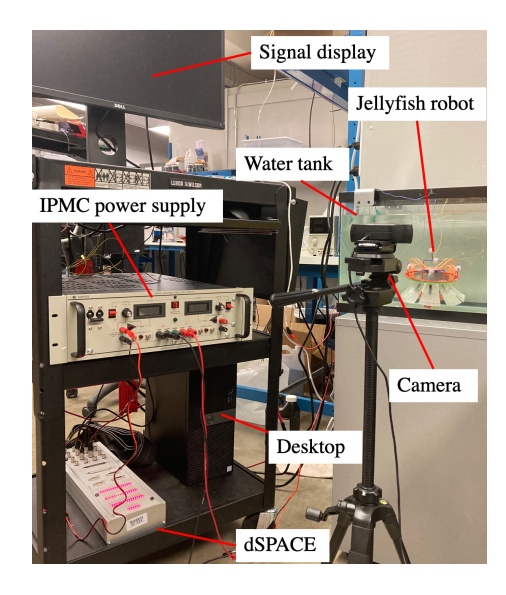


Fig. 9: Velocity measurement setup.

TABLE I: Velocity of jellyfish robot with frequency.

Time				
Frequency (Hz)	Contraction time (s)	Relaxation time (s)	Spending time (s)	Velocity (mm/s)
1.0	0.5	0.5	infinity	0
1.2	0.42	0.42	220	1.09
1.4	0.36	0.36	50	4.80
1.6	0.31	0.31	56	4.29
1.8	0.28	0.28	98	2.45
2.0	0.25	0.25	125	1.92

The experiment result shows that the speed of the jellyfish increases when frequency is increased from 1.0 Hz to 1.4 Hz, then decreases with increasing frequency. The time taken for the DE actuation response will be much less when the frequency is increased too much, the deflection of the DE per cycle will reduce. There are reduction of deflection in each cycle under high frequency [27] and unsubstantial speed increase when approaching 1.4 Hz. So 1.4 Hz is the optimal frequency among the six experiments.

# C. Direction Change with Actuation of IPMC

Another group of experiments with IPMC is documented on camera. The type of IPMC power supply is BOP 20-20D (KEPCO Inc.), which can provide voltage from -20 V to 20 V. The absolute value of voltage is taken in the range of 5 V to 7 V. The experiment results recorded by the camera shown in Fig. 10. The green big O-ring is chose as the reference to get the heading angle of the jellyfish robot. At different moments, a yellow line can be found which is perpendicular to the seam line of the O-ring. At t=0 s, the yellow line represents the original heading angle, which is  $0^{\circ}$ . In Fig. 10, the right line is the maximize heading angle when negative voltage is applied, there is an exception for 7 V. The left line is the left maximize heading angle when positive voltage is applied.

Five groups of experiments are conducted using different actuation voltages on IPMC. OpenCV is used to read each of

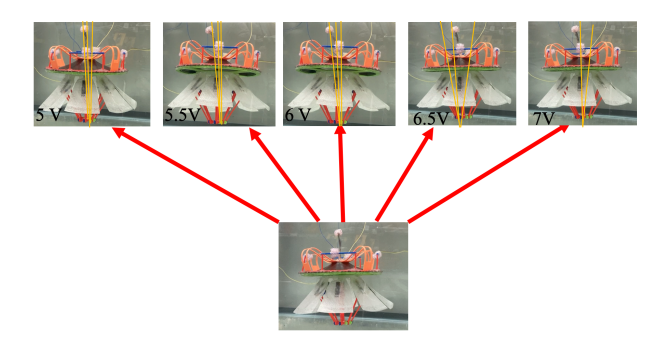


Fig. 10: Direction change by IPMC.

TABLE II: Heading angle change by actuating IPMC

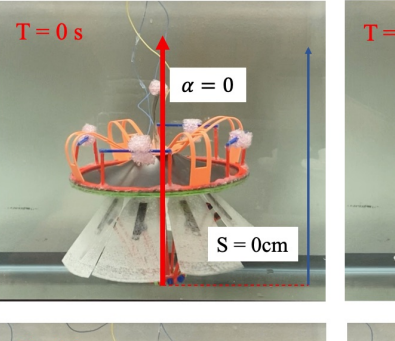
	Heading angle		
Voltage $(V)$	Left angle (°)	Right angle (°)	Average angle (°)
5	1.01	3.02	2.01
5.5	3.68	1.35	2.51
6	4.02	2.01	3.02
6.5*	12.07	5.03	8.55
7*	7.04	0	3.52

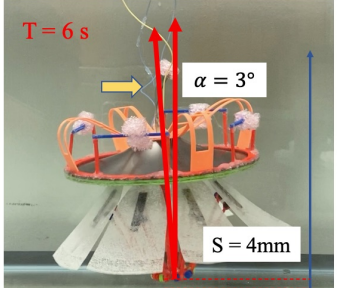
images. The angle between certain lines can be calculated with <code>hough\_line\_peaks</code> package in Python. The positive voltage will drive IPMC to bend to the right. Then the heading angle of the jellyfish will change to left side. Similarly, the negative voltage will drive IPMC to bend to the left. Then the heading angle of the jellyfish will change to right side. The average angle change is summarized in Table. II.

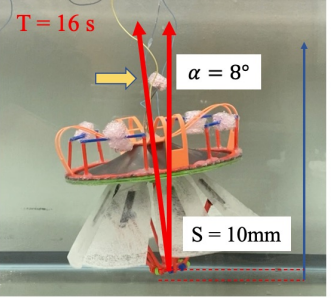
The results show the change of heading angle will increase with the voltage applied on IPMC increased from 5 V to 6.5 V. However, when the actuation voltage is increased to 6.5 V or above, IPMC produces lots of bubble, which interferes the behavior of DE membrane. Since we seal the IPMC inside of VHB tape, the bubbles will also be sealed inside of VHB, then they will destroy the balance of the whole jellyfish robot. As we can see from the last experiment with 7 V actuation voltage, there is no heading angle change. One of the main reasons is that the IPMC produced lots of bubbles on both sides of IPMC membrane. Even though the IPMC changed the position of foam, the buoyancy produced by the bubbles still keeps the robot in the vertical direction. The bubbles can also improve the performance of IPMC if the bubbles converge on one side of IPMC, like the experiment with 6.5 V actuation voltage. But this can lead to experimental instability.

The last experiment has been performed for evaluating the performance of the jellyfish robot by combing DE membrane and IPMC. Based on previous two experiments, the optimal actuation signal for DE is sinusoidal wave with 5 kV amplitude and 1.4 Hz frequency, for IPMC is 6 V actuation voltage. The maximum bending angle of IPMC with a foam fixed on its top is around  $30^{\circ}$  in the water. The movement of robot shown in Fig. 11. In the first picture, t = 0 s, the jellyfish robot was at negative buoyancy, and stayed in the bottom of the water tank. After the voltage was applied on DE, the jellyfish started to move upward. At the same time, 6 V voltage was applied on the IPMC. The IMPC started bending to right side at certain

angle. The body of the jellyfish robot tilted to left side. The robot was still moving upward, so the overall moving direction is upper left.







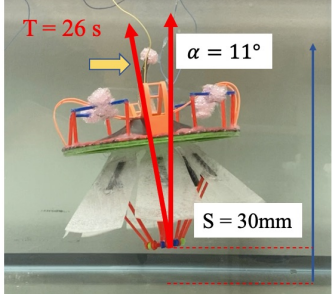


Fig. 11: Movement of jellyfish robot.

# D. Verification of Heading Angle Model

The experimental data were obtained for an IPMC actuator with dimensions 40 mm  $\times$  20 mm  $\times$  0.36 mm. The detailed physical models have been introduced in Section III, parts of the simulation parameters are listed in Table III and Table IV [28]. The actuation-induced bending moment  $M_{IPMC}$  can be estimated by the Final value theorem  $\lim_{t\to\infty} f(t) = \lim_{s\to 0} sF(s)$  with the input voltage between 4.9 V to 6.1 V.

Fig. 12 shows the heading angle versus the input voltage to IPMC. The dark blue line is the simulation result, the triangles mark different experimental results in IV-C, the red stars are the average heading angles. The simulation results are within the range of experimental data. As the input voltage to IPMC gets relatively bigger, the heading angle of the jellyfish robot increases.

TABLE III: Parameters of jellyfish robot

Parameters	Value	Parameters	Value
$F_{b_{foam}}$	0.0294 N	$F_{b_{jellyfish}}$	0.6566 N
Mass, m	73 g	$l_{hi}$	20 mm
E	1.2 GP	$l_{bh}$	3 mm
$l_{ab}$	37 mm	W	20 mm
L	40 mm	Density, $\rho$	$997 \text{ kg/m}^3$
Gravity, $g$	$9.81 \text{ m/s}^2$	,	C,

# V. CONCLUSION AND FUTURE WORK

A bio-inspired jellyfish robot based on dielectric elastomer material and IPMC is developed in this paper. With the help of the performance of DE material and position control of

TABLE IV: Parameters of electrical dynamics of IPMC

Parameters	Value	Parameters	Value
$\overline{F}$	96480 c/mol	T	300 K
R	8.314 J/(mol·K)	C-	$1090 \text{ mol/m}^3$
d	$5.4 \times 10^{-9}$	$k_e$	$2.48 \times 10^{-5}$ F/m
$lpha_0$	0.08 J/C mm		

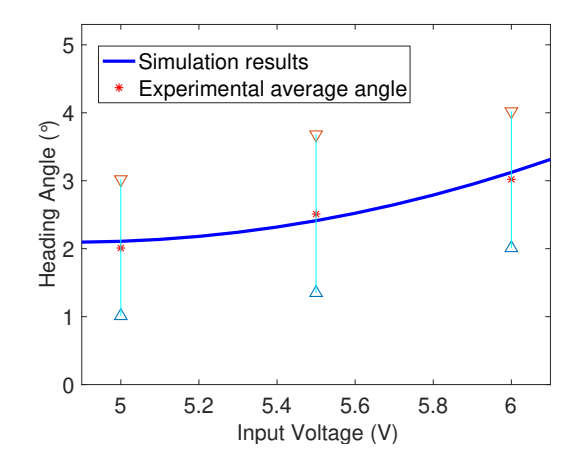


Fig. 12: Simulation results and experiment data.

foam with IPMC, the jellyfish robot can mimic the swimming mechanism to move forward and change direction in 2D plane. The swinging of the eight fins of the jellyfish robot can be accomplished by applying the sinusoidal voltage on the DE membrane. A physical model, based on the simplified jellyfish structure, incorporated with DE model and fin model is proposed to analyze the actuation mechanism of the robot. The preliminary experiment results have shown that the soft robot with multi-layer DE membranes can move effectively in water. The performance of the jellyfish is dependent on many factors, such as the frequency of the input signal, amplitude of voltage applied on IPMC.

In the further research, the behavior of the jellyfish under different types of signals will be explored. Developing a stabler model to capture different kinds of input signal, increasing the speed of the jellyfish, and controlling the movement direction as well as the speed of the jellyfish will also be studied in future work. Some robot-jelly enabled applications, such as underwater mobile sensing networks, will be explored.

# REFERENCES

- [1] J. Yuh, "Design and control of autonomous underwater robots: A survey," *Autonomous Robots*, vol. 8, no. 1, pp. 7–24, 2000.
- [2] B. Gemmell, K. Du Clos, S. Colin, K. Sutherland, and J. Costello, "The most efficient metazoan swimmer creates a 'virtual wall' to enhance performance," *Proceedings of the Royal Society B: Biological Sciences*, vol. 288, p. 20202494, 01 2021.
- [3] C. Christianson, C. Bayag, G. Li, S. Jadhav, A. Giri, C. Agba, T. Li, and M. T. Tolley, "Jellyfish-inspired soft robot driven by fluid electrode dielectric organic robotic actuators," *Frontiers in Robotics and AI*, vol. 6, p. 126, 2019.
- [4] C. Cruz Ulloa, S. Terrile, and A. Barrientos, "Soft underwater robot actuated by shape-memory alloys "jellyrobcib" for path tracking through fuzzy visual control," *Applied Sciences*, vol. 10, no. 20, p. 7160, 2020.

- [5] Z. Ren, W. Hu, X. Dong, and M. Sitti, "Multi-functional soft-bodied jellyfish-like swimming," *Nature communications*, vol. 10, no. 1, pp. 1–12, 2019.
- [6] C. Yin, F. Wei, S. Fu, Z. Zhai, Z. Ge, L. Yao, M. Jiang, and M. Liu, "Visible light-driven jellyfish-like miniature swimming soft robot," ACS Applied Materials & Interfaces, 2021.
- [7] J. Frame, N. Lopez, O. Curet, and E. D. Engeberg, "Thrust force characterization of free-swimming soft robotic jellyfish," *Bioinspiration* & *biomimetics*, vol. 13, no. 6, p. 064001, 2018.
- [8] S. P. Colin and J. H. Costello, "Morphology, swimming performance and propulsive mode of six co-occurring hydromedusae," *Journal of experimental biology*, vol. 205, no. 3, pp. 427–437, 2002.
- [9] M. Shahinpoor and K. Kim, "The effect of surface-electrode resistance on the performance of ionic polymer-metal composite (ipmc) artificial muscles," *Smart Materials and Structures*, vol. 9, p. 543, 08 2000.
- [10] L. Shi, S. Guo, and K. Asaka, "Development of a new jellyfish-type underwater microrobot." I. J. Robotics and Automation, vol. 26, 01 2011.
- [11] S.-W. Yeom and I.-K. Oh, "A biomimetic jellyfish robot based on ionic polymer metal composite actuators," *Smart Materials and Structures*, vol. 18, p. 085002, 06 2009.
- [12] J. Najem, A. Sarles, B. Akle, and D. Leo, "Biomimetic jellyfish-inspired underwater vehicle actuated by ionic polymer metal composite actuators," Smart Materials Structures SMART MATER STRUCT, vol. 21, 09 2012.
- [13] K. Mallavarapu, K. Newbury, and D. Leo, "Feedback control of the bending response of ionic polymer-metal composite actuators," *Proceed-ings of SPIE - The International Society for Optical Engineering*, vol. 4329, 07 2001.
- [14] J. Shintake, H. Shea, and D. Floreano, "Biomimetic underwater robots based on dielectric elastomer actuators," in *Proc. of 2016 IEEE/RSJ International Conference on Intelligent Robots and Systems*, 10 2016, pp. 4957–4962.
- [15] L. Maffli, S. Rosset, M. Ghilardi, F. Carpi, and H. Shea, "Ultrafast all polymer electrically tunable silicone lenses," *Advanced Functional Materials*, vol. 25, 03 2015.
- [16] J. Frame, N. Lopez, O. Curet, and E. Engeberg, "Thrust force characterization of free swimming soft robotic jellyfish," *Bioinspiration and Biomimetics*, vol. 13, p. 064001, 09 2018.
- [17] S. Wang, T. Kaaya, and Z. Chen, "Self-sensing of dielectric elastomer tubular actuator with feedback control validation," *Smart Materials and Structures*, 05 2020.
- [18] C. Christianson, C. Bayag, G. Li, S. Jadhav, A. Giri, C. Agba, T. Li, and M. Tolley, "Jellyfish-inspired soft robot driven by fluid electrode dielectric organic robotic actuators," *Frontiers in Robotics and AI*, vol. 6, p. 126, 11 2019.
- [19] G. Hareesh, J. Li, Y. Wang, and J. Zhu, "A soft jellyfish robot driven by a dielectric elastomer actuator," *IEEE Robotics and Automation Letters*, vol. 1, pp. 1–1, 07 2016.
- [20] T. Cheng, G. Li, Y. Liang, M. Zhang, B. Liu, T. W. Wong, J. Forman, M. Chen, G. Wang, Y. Tao, and T. Li, "Untethered soft robotic jellyfish," *Smart Materials and Structures*, vol. 28, 11 2018.
- [21] S. Wang and Z. Chen, "Modeling of jellyfish-inspired robot enabled by dielectric elastomer," *International Journal of Intelligent Robotics and Applications*, pp. 1–13, 2021.
- [22] M. Hodgins, A. York, and S. Seelecke, "Experimental comparison of bias elements for out-of-plane deap actuator system," *Smart Materials and Structures*, vol. 22, p. 094016, 08 2013.
- [23] M. Sfakiotakis, D. M. Lane, and J. B. C. Davies, "Review of fish swimming modes for aquatic locomotion," *IEEE Journal of oceanic* engineering, vol. 24, no. 2, pp. 237–252, 1999.
- [24] Q.-L. Zhao, J. Chen, H. Zhang, Z. Zhang, Z. Liu, S. Liu, J. Di, G. He, L. Zhao, M. Zhang et al., "Hydrodynamics modeling of a piezoelectric micro-robotic fish with double caudal fins," *Journal of Mechanisms and Robotics*, pp. 1–24, 2021.
- [25] D. Costa, M. Franciolini, G. Palmieri, A. Crivellini, and D. Scaradozzi, "Computational fluid dynamics analysis and design of an ostraciiform swimming robot," in 2017 IEEE International Conference on Robotics and Biomimetics (ROBIO). IEEE, 2017, pp. 135–140.
- [26] Z. Chen and X. Tan, "A control-oriented and physics-based model for ionic polymer–metal composite actuators," *IEEE/ASME Transactions On Mechatronics*, vol. 13, no. 5, pp. 519–529, 2008.
- [27] A. Kumar and R. Srivastava, "Modeling and simulation of a micropump chip using dielectric elastomer," in *International Journal of Engineering* Science and Innovative Technology, vol. 2, 2013.
- [28] Z. Chen, S. Shatara, and X. Tan, "Modeling of biomimetic robotic fish propelled by an ionic polymer–metal composite caudal fin," *IEEE/ASME* transactions on mechatronics, vol. 15, no. 3, pp. 448–459, 2009.



Shengbin Wang is a PhD student in the Mechanical Engineering Department at the University of Houston. He was born in Hubei, China. He received his MS degree in Mechanical engineering from the HeFei University of Technology, and BS degree in Mechanical Manufacturing and Automation from the Huazhong Agricultural University, China in 2018 and 2015, respectively. During his free time, he likes hiking and traveling around the world. His research is focused on neural-network based self-sensing of dielectric elastomer and electroactive polymer en-

abled bio-inspired underwater robots.



Zheng Chen was born in Hengyang, China. He received B.E. degree in electrical engineering and M.E. degree in control science and engineering from Zhejiang University, Hangzhou, China, in 1999 and 2002, respectively, and Ph.D. degree in electrical engineering from Michigan State University, East Lansing, MI, USA, in 2009. He was a Research Associate with the University of Virginia, Charlottesville, VA, USA, from 2009 to 2012, a Research and Development Engineer specializing in control systems with Baker Hughes from 2012 to 2013,

and an Assistant Professor of Electrical Engineering and Computer Science with Wichita State University, Wichita, KS, USA, from 2013 to 2017. He is currently an Assistant Professor of Mechanical Engineering with the University of Houston, Houston, TX, USA. His current research interests include dynamic systems and control, smart material sensors and actuators, and bio-inspired underwater robots. Dr. Chen received the First Award from the Kansas NSF EPSCoR in 2016 and the NSF CAREER Award in 2017.